PAPER

Superoscillatory behavior in partially coherent fields

View the article online for updates and enhancements.

IOP ebooks™

Bringing together innovative digital publishing with leading authors from the global scientific community.

Start exploring the collection–download the first chapter of every title for free.

Superoscillatory behavior in partially coherent fields

Joseph Mays and Greg Gbur

Department of Physics and Optical Science, UNC Charlotte, Charlotte, NC 28223,
United States of America

E-mail: gjgbur@uncc.edu

Abstract

Superoscillations are oscillations of a wavefield that are locally higher than the bandlimit of the field. Superoscillations have to date been studied primarily in coherent wavefields; here we look at superoscillations that appear in the phase of the correlation function in partially coherent fields. It is shown that a decrease in spatial coherence can in some cases strengthen the superoscillatory behavior, and in others decrease it. Superoscillations are studied in a number of model partially coherent fields, and the influence of coherence on each model is considered.

(Some figures may appear in colour only in the online journal)

1. Introduction

It is now widely recognized that band-limited signals can possess regions where the local frequency is arbitrarily larger than the fastest oscillating Fourier component in the function. The oscillations in these regions are known as *superoscillations* [1, 2]. The local rate of oscillation of a real-valued signal is often dictated by the separation of its zeros, with the space between two zeros representing one half of an oscillation; when the space is less than one half of a wavelength, the field in the region is said to be superoscillatory.

Superoscillations have been demonstrated by a number of mathematical techniques, but perhaps the simplest of these was done by Chremmos and Fikioris [3], who showed that zeros can be moved arbitrarily close together in a bandlimited function without any effect on the bandlimit; a similar construction was used to design superoscillations in the cross-section of a complex monochromatic optical field [4]. In such complex fields, superoscillations may be directly connected to the presence of optical vortices, lines in three-dimensional space around which the field has a circulating or helical structure [5]. The creation of superoscillations may therefore be viewed as the control and manipulation of optical vortices and other field singularities.

As the superoscillatory zeros are moved closer together, the amplitude of the oscillations between them decreases.

Furthermore, the superoscillatory region is inevitably surrounded by regions where the amplitude is significantly larger, becoming orders of magnitude larger even for modest gains in local frequency. Though at first glance this would appear to make superoscillations impractical, a number of researchers have designed and tested superoscillation-based lenses that can improve the resolution of imaging systems through the creation of subwavelength spots [6–10]. Superoscillations have therefore become of practical as well as scientific interest.

When a field possesses fluctuations in space and time, i.e. it is partially coherent, zeros of intensity typically disappear [11]. This in turn suggests that the superoscillatory behavior breaks down, as has been demonstrated in several studies [12, 13]. Though coherent optical vortices disappear as the coherence is decreased, analogous structures can appear in the correlation functions of partially coherent fields. These *correlation vortices* or *coherence vortices* appear in the phase of a two-point correlation function when one observation point is fixed [14, 15]; it has also been recognized that optical vortices evolve into correlation vortices as the spatial coherence of a vortex beam is decreased [16].

With these observations in mind, it is clear that superoscillations must also appear in partially coherent fields and, considering the numerous applications of partially coherent fields [17], it is natural to wonder whether superoscillations in correlation functions can also be applied to optical problems. In this

paper, we study superoscillations in partially coherent light using a number of models of partially coherent beams possessing vortex structures. We begin by considering the randomization of a coherent beam possessing superoscillations, and are led to other possibilities. The dependence of superoscillations on the correlation length of the source is studied, and we present some general remarks on the relationship between superoscillations and coherence.

2. Coherence theory and singularities

To characterize fields that possess random fluctuations, it is necessary to study the average properties of the field, in particular two-point correlation functions. Throughout this paper we will use the cross-spectral density, which can be defined as [18]:

$$W(\mathbf{r}_1, \mathbf{r}_2, \omega) = \langle \tilde{U}(\mathbf{r}_1, \omega) U(\mathbf{r}_2, \omega) \rangle_\omega, \tag{1}$$

where $U(\mathbf{r}, \omega)$ represents a monochromatic scalar field and $\langle \cdots \rangle_\omega$ represents an average over an ensemble of monochromatic fields. For convenience, we use a tilde to represent the complex conjugate throughout the paper. The spectral density of the field, or intensity at frequency ω, can be found from the cross-spectral density with $\mathbf{r}_1 = \mathbf{r}_2 = \mathbf{r}$,

$$S(\mathbf{r}, \omega) = W(\mathbf{r}, \mathbf{r}, \omega). \tag{2}$$

One particularly important feature of the cross-spectral density is that it satisfies a pair of Helmholtz equations in the spatial variables $\mathbf{r}_1$ and $\mathbf{r}_2$,

$$\begin{aligned} \Delta_1^2 W(\mathbf{r}_1, \mathbf{r}_2, \omega) + k^2 W(\mathbf{r}_1, \mathbf{r}_2, \omega) = 0, \\ \Delta_2^2 W(\mathbf{r}_1, \mathbf{r}_2, \omega) + k^2 W(\mathbf{r}_1, \mathbf{r}_2, \omega) = 0, \end{aligned} \tag{3}$$

where Δ_1 represents the Laplacian with respect to $\mathbf{r}_1$, and so forth. When $\mathbf{r}_1$ is held fixed, the cross-spectral density will propagate like a monochromatic wave with respect to $\mathbf{r}_2$. As we know that optical vortices are common within monochromatic fields, the cross-spectral density with one position vector fixed should manifest vortices as well, which are referred to as correlation vortices. These vortices are generic features for the cross spectral density.

We will be displaying and referring to vortex structures throughout the body of this paper. A vortex, in a field or a correlation function, can be identified as a point where all phase values converge. Though we have qualitatively described the structure of an optical vortex, it is convenient to provide a visual example as well. Figure 1 displays the intensity and the phase in the cross-section of a Laguerre–Gauss (LG) beam of radial order $n = 0$ and azimuthal order $m = 1$ in the waist plane of the beam; LG beams of non-zero azimuthal order possess a zero line on their propagation axis and possess a vortex structure around that axis. It can be clearly seen that the phase increases by 2π as one follows a counterclockwise path around the vortex core. For a correlation function, the phase represents the absolute position of fringes as measured in a wavefront splitting interferometer such as Young's interferometer.
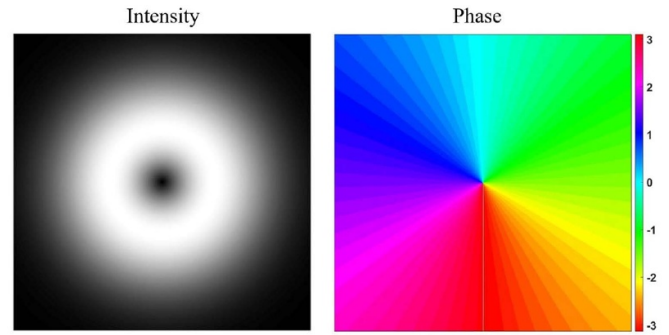
Figure 1. The intensity and phase of a first order vortex within a Laguerre–Gauss beam of radial order $n = 0$ and azimuthal order $m = 1$.

It is to be noted that the strength of superoscillations is often characterized by a local wavenumber [19], which for the cross-spectral density is defined by the expression,

$$k(\mathbf{r}_1, \mathbf{r}_2) = \left| Im \frac{\nabla_{\mathbf{r}_2} W(\mathbf{r}_1, \mathbf{r}_2)}{W(\mathbf{r}_1, \mathbf{r}_2)} \right|. \tag{4}$$

This quantity measures rapid oscillations of the complex phase of a wavefield; however, the models we will introduce typically produce close-packed zeros, with a constant phase between them, and the local wavenumber is not optimal for characterizing the behavior. Throughout this paper we monitor the superoscillatory behavior through measuring the separation distance between the singularities.

3. Partially coherent superoscillations

We are interested in exploring how altering the spatial coherence of a field affects any superoscillatory behavior contained in the field. We take the natural first step of setting up a coherent field that already contains superoscillations and study how this behavior changes as the spatial coherence is decreased.

We model a randomized superoscillatory field using what is known as the beam wander model [11]. In this model, the axis of propagation of a paraxial beam is treated as a random function of transverse position. The cross spectral density of such a field may be written as:

$$W(\mathbf{r}_1, \mathbf{r}_2) = \int \tilde{U}(\mathbf{r}_1 - \mathbf{r}_0) U(\mathbf{r}_2 - \mathbf{r}_0) f(\mathbf{r}_0) d^2 \mathbf{r}_0, \tag{5}$$

with $f(\mathbf{r}_0)$ being the probability density for the position of the axis and $\mathbf{r}_0$ being the transverse position on the axis, such that:

$$f(\mathbf{r}_0) = \frac{1}{\pi \delta^2} \exp \left[-\frac{(x_0^2 + y_0^2)}{\delta^2} \right], \tag{6}$$

with $|\mathbf{r}_0|^2 = x_0^2 + y_0^2$ and δ represents the wander radius of the axis.
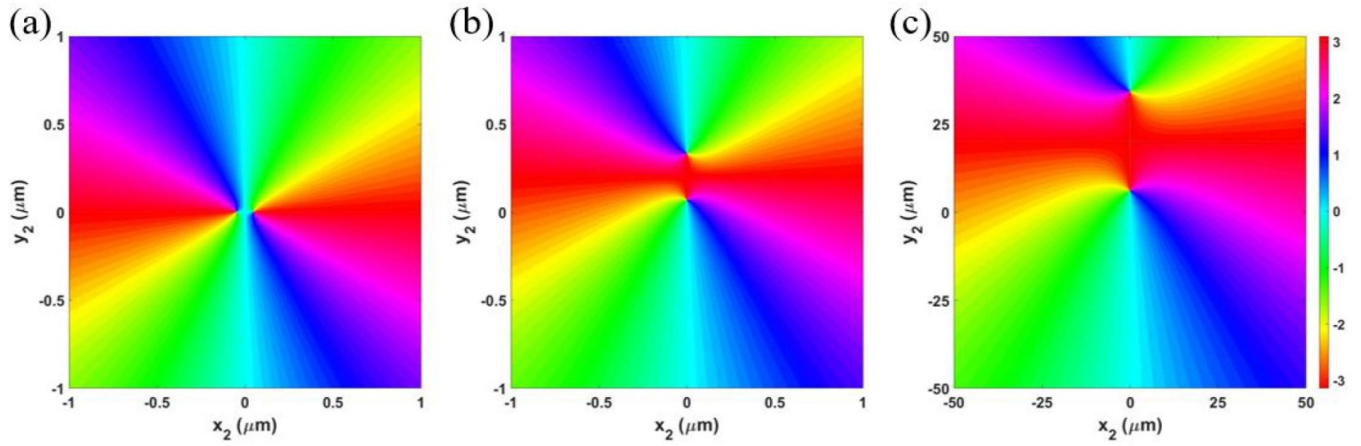
Figure 2. Phase of the cross-spectral density of two closely spaced vortices using the beam wander model. For each of the images above, $\lambda = 500$ nm, $(x_1, y_1) = (0.0, 1000)$ μm, $\sigma = 5$ mm, and $\Delta = 0.1$ λ. The wander radius δ and corresponding vortex separation distance α are (a) $\delta = 1$ μm and $\alpha = 0.1$ μm, (b) $\delta = 10$ μm and $\alpha = 0.27$ μm, (c) $\delta = 100$ μm and $\alpha = 28.3$ μm. The plot range in (c) is increased to accommodate the very large vortex separation.

To study a partially coherent field possessing superoscillations, we choose for $U(\mathbf{r})$ the form,

$$U(\mathbf{r}) = (z + \Delta)(z - \Delta)\exp\left[-\frac{r^2}{2\sigma^2}\right], \qquad (7)$$

where $z = x + iy$, σ is the beam width, and Δ is the complex spacing of the pair of vortices built into the function. In this model, δ is inversely related to the field coherence: a smaller delta corresponds to a more coherent field. We use a Gaussian beam for mathematical convenience; however, it is to be noted that a Gaussian function is not strictly bandlimited. Within the context of the paraxial approximation, a choice of Δ smaller than one quarter of the wavelength (with less than one half of a wavelength between the zeros) will accurately approximate superoscillatory behavior. The relationship between such 'leaky' functions and superoscillations has been explored in depth elsewhere [20].

The integral of equation (5) is evaluated in appendix A. The final result for the cross-spectral density may be written as:

$$W(\mathbf{r}_1, \mathbf{r}_2) = Q_1\left[\frac{1}{A^3} + \frac{2\tilde{C}_1 C_2}{A^2} + \frac{\tilde{D}_1 D_2}{2A}\right], \qquad (8)$$

where

$$A = \frac{1}{\sigma^2} + \frac{1}{\delta^2}, \qquad (9)$$

$$\tilde{D}_1 = \tilde{C}_1^2 - \Delta^2, \quad D_2 = C_2^2 - \Delta^2, \qquad (10)$$

$$C_i = C_{ix} + iC_{iy}, \qquad (11)$$

$$C_{1x} = x_1 - \frac{\frac{x_1}{\tilde{\sigma}^2} + \frac{x_2}{\sigma^2}}{2A}, \quad C_{2x} = x_2 - \frac{\frac{x_1}{\tilde{\sigma}^2} + \frac{x_2}{\sigma^2}}{2A},$$
$$C_{1y} = y_1 - \frac{\frac{y_1}{\tilde{\sigma}^2} + \frac{y_2}{\sigma^2}}{2A}, \quad C_{2y} = y_2 - \frac{\frac{y_1}{\tilde{\sigma}^2} + \frac{y_2}{\sigma^2}}{2A}. \qquad (12)$$

The constant Q_1 is defined in equation (38). It is a combination of Gaussian functions which possess no zeros, and can be neglected in the study of superoscillations.

We now consider how the position of the superoscillatory vortex pair changes as the spatial coherence of the field is decreased. We study the vortex structure of the correlation function by holding position vector $\mathbf{r}_1$ fixed and evaluating the phase of the cross-spectral density with respect to $\mathbf{r}_2$. This phase is plotted in figure 2 for several values of δ, starting with the vortices separated by 0.1λ. As the coherence is decreased, the separation distance between the two vortices increases, reaching a half-wavelength separation when the wander radius approaches 10 μm. Furthermore, the vortices transition to being aligned along the y-axis instead of the x-axis, in line with the reference point. As can be seen in figure 2(c), the distance between vortices continues to increase as the wander radius increases.

Qualitatively similar behavior arises when the reference point $\mathbf{r}_1$ is moved to other locations at a comparable radial distance from the beam axis, though the orientation of the vortices changes. For example, if the reference point is rotated to the x-axis, the vortices still separate as the spatial coherence is decreased, but they align along the x-axis, again in line with the reference point.

Though the preceding example indicates that the superoscillatory behavior is degraded as spatial coherence is decreased, it can be at least partly recovered if the reference point is moved significantly beyond the wander radius. Figure 3 shows the change in the vortex position as $\mathbf{r}_1$ is moved further from the axis. It can be seen that the correlation vortices, which had separated and moved to a vertical line, move back together along a horizontal line with increasing $|\mathbf{r}_1|$, looking very much like the decrease of spatial coherence has been reversed by moving the observation point.

We may interpret this effect as follows. The overall structure of the correlation function depends on the random fluctuations at both $\mathbf{r}_1$ and $\mathbf{r}_2$, and the correlations between them. As we move $\mathbf{r}_1$ outside the wander radius, the fluctuations of
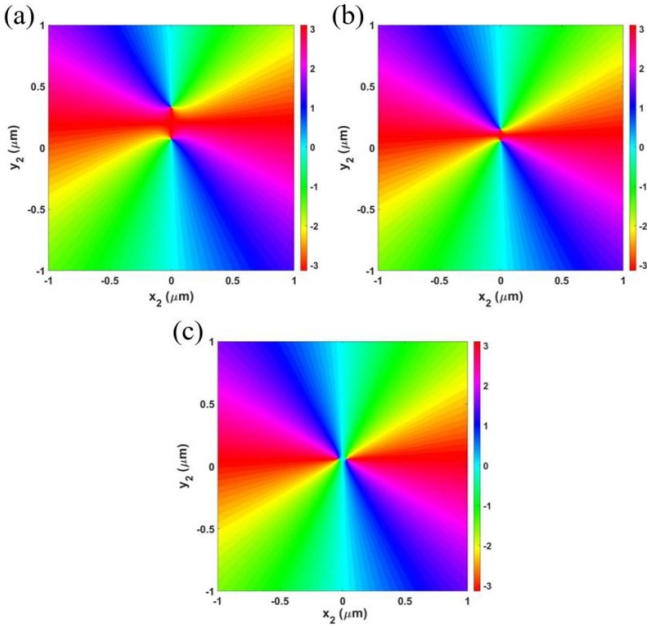
Figure 3. Phase of the cross-spectral density of two closely spaced vortices using the beam wander model. For each of the images above, $\lambda = 500$ nm, $\delta = 10$ μm, $\sigma = 5$ mm, and $\Delta = 0.1\,\lambda$. The reference point position and corresponding vortex separation distance α are (a) $(x_1, y_1) = (0.0, 1000)$ μm and $\alpha = 0.27$ μm, (b) $(x_1, y_1) = (0.0, 2000)$ μm and $\alpha = 0.105$ μm, (c) $(x_1, y_1) = (0.0, 4000)$ μm and $\alpha = 0.07$ μm.
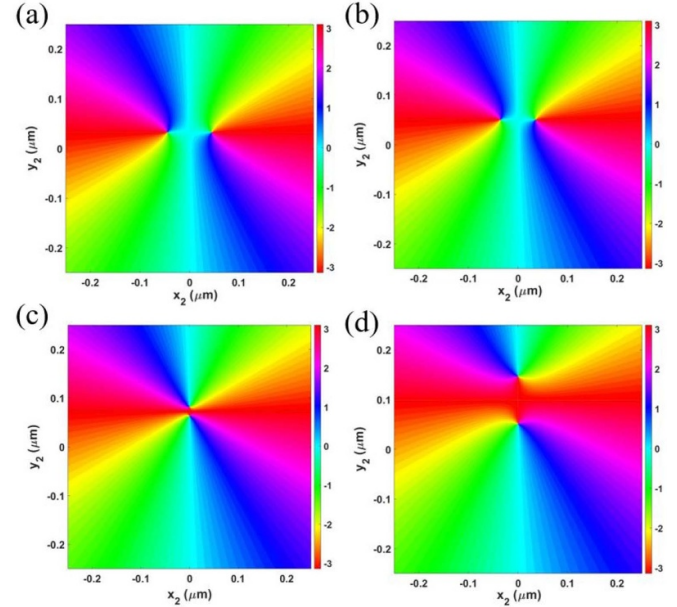
Figure 4. Phase of the cross-spectral density of two closely spaced vortices as the spatial coherence is incrementally lowered. For each of the images above, $\lambda = 500$ nm, $(x_1, y_1) = (0.0, 1000)$ μm, $\sigma = 5$ mm, and $\Delta = 0.1\,\lambda$. The wander radius δ and corresponding vortex separation distance α are (a) $\delta = 4$ μm and $\alpha = 0.089$ μm, (b) $\delta = 5$ μm and $\alpha = 0.071$ μm, (c) $\delta = 6$ μm and $\alpha = 0.019$ μm, and (d) $\delta = 7$ μm and $\alpha = 0.096$ μm.

the field at this point are greatly reduced, resulting in the overall field appearing more coherent. This observation indicates that, with an appropriate choice of observation point, we may maintain the superoscillatory behavior of the field even as the spatial coherence decreases. It is to be noted that the position of $\mathbf{r}_1$ still lies within the beam radius of $\sigma = 5$ mm, so the field intensity at this point is still appreciable.

In both figures 2 and 3, the vortices change their orientation with respect to the origin. It is natural to ask how the separation distance of the vortices evolves as this transition occurs, and this is illustrated for a change of δ in figure 4. As we incrementally increase the wander radius, the singularities in fact come closer together at first, meaning that a decrease in partial coherence has enhanced the superoscillatory behavior. The singularities reach a minimum non-zero separation before moving along the vertical axis. It is to be noted that this enhancement occurs only for a small range of wander radii δ; however, this shows that the randomization of a field, under the right circumstances, can decrease the separation distance between two singularities.

4. Partially coherent superoscillations from higher-order vortex beams

The first example above indicates that, outside of small range of δ values, a decrease in spatial coherence tends to

increase the spacing between correlation vortices in a wavefield. We may use this observation, however, as a strategy to produce superoscillations in a partially coherent field from a higher-order vortex beam. It is well-known that higher-order vortices are unstable, non-generic, features of a wavefield that will break into a collection of first-order vortices under wavefield perturbations. Such perturbations include a decrease in spatial coherence, as has been shown in [21]. Thus we can make a superoscillatory partially coherent field by perturbing a higher-order vortex beam, as we illustrate next.

We consider the randomization of a second-order LG beam, of order $n = 0$, $m = 2$, of the form:

$$
\begin{aligned}
U_{0,2}^{LG}(x,y) = &\sqrt{\frac{2}{2\pi\sigma^2}} \left(\frac{\sqrt{2}}{\sigma} \right)^2 (x \pm iy)^2 \\
&\times \exp\left[-\frac{1}{\sigma^2}(x^2 + y^2) \right],
\end{aligned}
\tag{13}
$$

where σ is the beam width at the waist plane $z = 0$. We use this beam in equation (5) to generate the cross-spectral density, which is a special case of the class of beams given in [22]. The cross-spectral density may be written as:
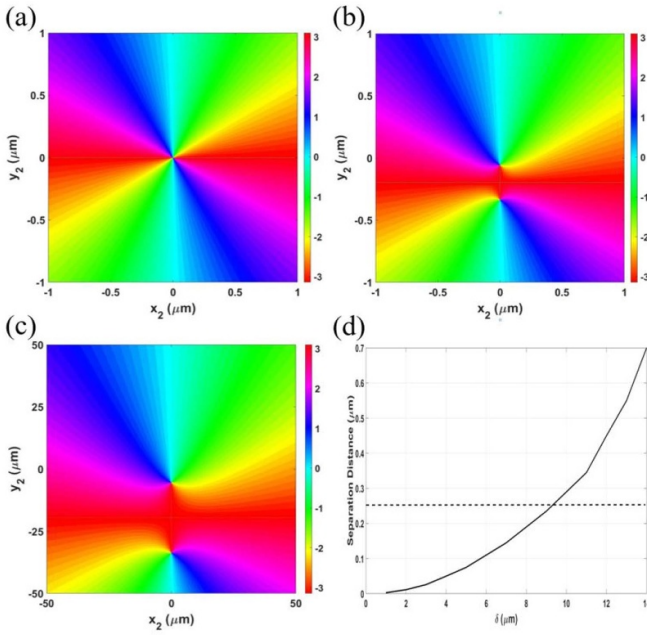
Figure 5. Phase of the cross-spectral density of a second order vortex and its subsequent first order vortices. For each of the images above, $\lambda = 500$ nm, $(x_1, y_1) = (0.0, 1000)$ μm, $\sigma = 5$ mm. In the figure: (a) $\delta = 1$ μm, (b) $\delta = 10$ μm, (c) $\delta = 100$ μm. (d) shows the relationship between the increase in wander radius (decrease in coherence), and the separation distance between the two singularities.

$$W(\mathbf{r}_1, \mathbf{r}_2) = \pi f(\mathbf{r}_1, \mathbf{r}_2) \left[\sum_{l=0}^{1} \binom{2}{l}^2 \frac{\Gamma(l+1)}{A^{4-l+1}} \right.$$
$$\times \left[\frac{1}{\alpha^2}(x_2 \pm iy_2) - \frac{1}{\sigma^2}(x_1 \pm iy_1) \right]^{2-l}$$
$$\times \left[\frac{1}{\alpha^2}(x_1 \mp iy_1) - \frac{1}{\sigma^2}(x_2 \mp iy_2) \right]^{2-l}$$
$$\left. + \frac{\Gamma(3)}{A^3} \right], \tag{14}$$

where A is the same as in equation (9), and

$$\frac{1}{\alpha^2} \equiv \left[\frac{1}{\sigma^2} + \frac{1}{\delta^2} \right]. \tag{15}$$

The quantity $f(\mathbf{r}_1, \mathbf{r}_2)$ represents the envelope of a Gaussian Schell-model beam as defined by:

$$f(\mathbf{r}_1, \mathbf{r}_2) \equiv \frac{|C|^2}{\pi \delta^2} \exp \left[-\frac{r_1^2}{A\delta^2 \tilde{\sigma}^2} \right] \exp \left[-\frac{r_2^2}{A\delta^2 \sigma^2} \right]$$
$$\times \exp \left[-\frac{|\mathbf{r}_1 - \mathbf{r}_2|^2}{A|\sigma|^4} \right]. \tag{16}$$

Figure 5 shows the phase of the cross-spectral density as a function of δ. In the coherent limit, the phase of the cross-spectral density manifests a single second-order vortex at the origin. As the coherence decreases, the second-order vortex separates into two first-order singularities that are very close together, exhibiting superoscillatory behavior. As with the

previous example, as the coherence is further decreased, the vortices will separate enough that they no longer represent superoscillations.

One particular point of interest is to look at the rate at which the two first-order singularities separate while still being superoscillatory. Figure 5(d) shows the relationship between the wander radius and the separation distance between the singularities. It is immediately apparent that it only requires a small decrease in coherence, with a wander radius much smaller than the beam width, to increase the separation distance to the point that we would no longer consider the field to be superoscillatory. This limit is shown as the dotted line in figure 5(d), which represents a half-wavelength separation distance. We used a wander radius of 1 μm to represent the coherent limit. For a wander radius of 9 μm, the vortex separation increases to approximately 250 nm, equal to a half-wavelength.

This example shows we can create superoscillations in a partially coherent field by decreasing the spatial coherence of a second-order vortex beam. If we use an even higher-order vortex beam, we can get a line of correlation vortices representing an extended region of superoscillatory behavior. Again, a change in the position of the observation point allows one to change the orientation of the line of vortices.

Here we have explicitly used the observation that a decrease of coherence in the beam wander model results in a decrease in superoscillatory behavior. This brings us to wonder if there are any scenarios in which a decrease in coherence can bring about an increase in superoscillatory behavior. This is explored in the next section.

5. Modal coherence model

The previous examples showed that superoscillatory behavior tends to decrease as the spatial coherence of a field is significantly lowered. However, this is not a universal behavior. It is possible to introduce fields for which the zero spacing decreases as the coherence is decreased, as we now show.

We again consider a field of two closely-spaced vortices modulated by a Gaussian envelope, as in equation (7). Again, Δ is the separation of the vortices, σ is the width of the Gaussian, and $z = x + iy$. The zeros are aligned along the y-axis for this case, so that Δ is pure imaginary.

We now rewrite equation (7) as a coherent superposition of LG beams of orders (0, 0) and (0, 2). The field then takes the form,

$$U(\mathbf{r}) = U_{02}(\mathbf{r}) - \Delta^2 U_{00}(\mathbf{r}), \tag{17}$$

where

$$U_{02}(\mathbf{r}) = z^2 \exp \left[-\frac{r^2}{2\sigma^2} \right], \tag{18}$$

and

$$U_{00}(\mathbf{r}) = \exp \left[-\frac{r^2}{2\sigma^2} \right]. \tag{19}$$
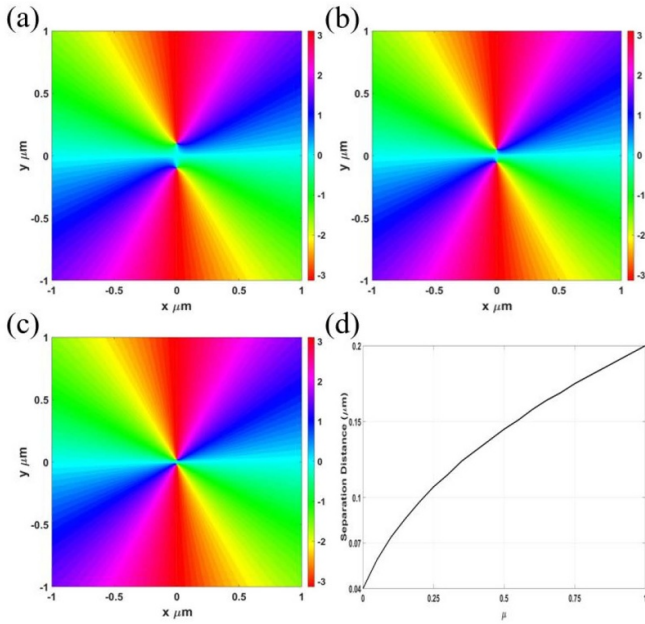
Figure 6. Phase of the cross-spectral density of two closely spaced vortices as a function of $\mathbf{r}_2$ with $\mathbf{r}_1 = (0.5, 0)$. Here $\Delta = 0.1i$ μm and $\sigma = 1$ μm. The degree of coherence and the corresponding separation distance α for the first three figures are (a) $\mu = 1$ and $\alpha = 0.2$ μm, (b) $\mu = 0.25$ and $\alpha = 0.1$ μm, (c) $\mu = 0$ and $\alpha = 0.02$ μm. (d) Relationship between the change in degree of coherence and the separation distance between the singularities.

We have left off the traditional normalization of the LG beams for simplicity. By treating our superoscillatory field as a superposition of LG beams, we can now explore the effect of reducing the spatial coherence between the beams. If we imagine that the overall coherence between the beams is characterized by the complex degree of coherence μ, we can find the cross-spectral density by taking the product of $\tilde{U}(\mathbf{r}_1)$ with $U(\mathbf{r}_2)$, and introducing the factor μ into the cross terms, giving the result,

$$
W(\mathbf{r}_1, \mathbf{r}_2) = \exp\left[-\frac{r_1^2}{2\sigma^2}\right] \exp\left[-\frac{r_2^2}{2\sigma^2}\right] \\
\times \left[\tilde{z}_1^2 z_2^2 - \tilde{\mu}\Delta^2 \tilde{z}_1^2 - \mu\tilde{\Delta}^2 z_2^2 + \tilde{\Delta}^2\Delta^2\right].
\tag{20}
$$

Figure 6 shows the phase of the cross-spectral density for decreasing values of μ, taken to be real for simplicity. The vortices, which are already superoscillatory for $\mu = 1$, move closer together as the degree of coherence is decreased: the superoscillatory behavior becomes stronger. Figure 6(d) shows that the zero spacing is 0.08 μm for $\mu = 0$, one sixth of a wavelength. This example demonstrates that a decrease of coherence can, under the right circumstances, create or strengthen superoscillations.

There is one significant advantage to be found in using partially coherent fields to produce superoscillations. Figure 7 displays the spectral density (intensity) of the field, as defined
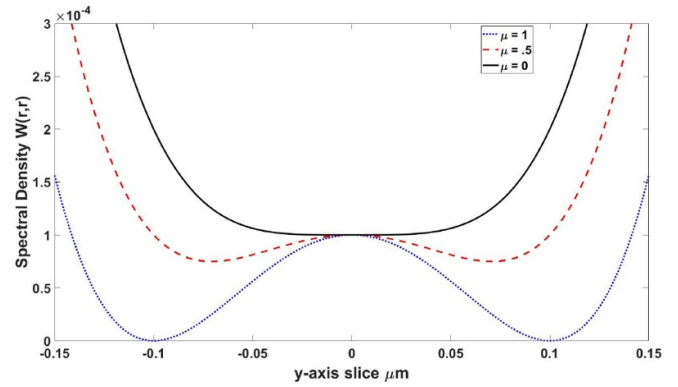
Figure 7. The spectral density S($\mathbf{r}$, ω) along the *y*-axis of two closely spaced vortices as a function of $\mathbf{r}_2 = \mathbf{r}_1 = \mathbf{r}$. Here $\Delta = 0.1i$ μm and $\sigma = 1$ μm.

in equation (2), along the *y*-axis as the degree of coherence is lowered. The zeros of intensity for the fully coherent field disappear as the spatial coherence is decreased, resulting in a uniform low, but non-zero, intensity in the region of the correlation vortices. Because correlation vortices do not have to appear at regions of zero intensity, it is possible to have appreciable light in a superoscillatory region, a strong difference from the coherent case. Though the intensity is still low for this example, more sophisticated examples might demonstrate superoscillatory correlation functions in regions of high intensity.

We noted earlier that we have been using beams which are only approximately bandlimited, i.e. 'leaky.' The modal model for a partially coherent superoscillatory beam presented here, however, is simple enough to be adapted to a true bandlimited field using Bessel beams. Noting that, for a small argument, a Bessel beam may be approximated by the form,

$$
J_n(x) \approx \frac{1}{n!}\left(\frac{x}{2}\right)^n,
\tag{21}
$$

we may construct a coherent field with zeros approximately at positions $\pm\Delta$ using the expression,

$$
U(\mathbf{r}) = -\Delta^2 J_0(\gamma r) + \frac{8}{\alpha^2} J_2(\gamma r)e^{2i\phi},
\tag{22}
$$

where γ may be identified as the inverse width of the Bessel beam. By assuming a degree of coherence μ between the zeroth and second order Bessel components of the field, we can again study how the superoscillations change as μ is decreased. We again chose $\mathbf{r}_1 = (0.5, 0)$, $\Delta = 0.1i$ μm, and $\lambda = 500$ nm as in figure 6. The quantity $\gamma = 5$ μm, which corresponds to a Bessel beam with an opening angle of $23°$. The evolution of the vortices of the correlation function matched the results of figure 6 almost exactly, showing that we get the same superoscillatory behavior for a true bandlimited function.

6. Modal coherence: radial case

For imaging applications, a superoscillatory spot created with a zero ring is preferable to a superoscillation created with a pair of point zeros. In 2020, for example, Smith and Gbur [10] demonstrated how to generalize the method of Chremmos and Fikioris [3] to produce a superoscillatory point-spread function using ring zeros. Here, we explore whether the modal coherence method of the previous section can be used to produce superoscillatory spots in the cross-spectral density.

We now work with LG modes of different radial order, which possess zero rings, instead of modes of different azimuthal order. We alter equations (17)–(19) to instead produce a zero ring at a radial position r_0. We have

$$U(r) = \frac{r_0^2 - r^2}{2\sigma^2} \exp\left[-\frac{r^2}{2\sigma^2}\right]$$

$$= U_{10}(r) - \left(1 - \frac{r_0^2}{2\sigma^2}\right) U_{00}(r), \quad (23)$$

$$U_{10}(r) = \left(1 - \frac{r^2}{2\sigma^2}\right) \exp\left[-\frac{r^2}{2\sigma^2}\right], \quad (24)$$

$$U_{00}(r) = \exp\left[-\frac{r^2}{2\sigma^2}\right]. \quad (25)$$

Taking these adjustments into account and utilizing the same process as the previous example. The cross-spectral density for the radial case can be show to be:

$$W(\mathbf{r}_1, \mathbf{r}_2) = \exp\left[-\frac{r_1^2}{2\sigma^2}\right] \exp\left[-\frac{r_2^2}{2\sigma^2}\right] \left[\left(1 - \frac{r_1^2}{2\sigma^2}\right)\right.$$
$$\times \left(1 - \frac{r_2^2}{2\sigma^2}\right) - \tilde{\mu}\left(1 - \frac{r_0^2}{2\sigma^2}\right)\left(1 - \frac{r_1^2}{2\sigma^2}\right)$$
$$\left. - \mu\left(1 - \frac{r_0^2}{2\sigma^2}\right)\left(1 - \frac{r_2^2}{2\sigma^2}\right) + \left(1 - \frac{r_0^2}{2\sigma^2}\right)^2\right]. \quad (26)$$

The radius of the zero ring can be determined the bracketed term of equation (26). If we set that term equal to zero and solve for r_2^2, we find the zero ring has a radius in r_2 given by:

$$r_2^2 = 2\sigma^2 \left[1 - \frac{\tilde{\mu}\left(1 - \frac{r_0^2}{2\sigma^2}\right)\left(1 - \frac{r_1^2}{2\sigma^2}\right) - \left(1 - \frac{r_0^2}{2\sigma^2}\right)^2}{\left(1 - \frac{r_1^2}{2\sigma^2}\right) - \mu\left(1 - \frac{r_0^2}{2\sigma^2}\right)}\right]. \quad (27)$$

This allows us to determine the spot size of this field for any values of r_1, r_0, and μ.

Figure 8 gives an example of the phase of the cross-spectral density as the coherence is decreased; the discontinuous jump represents the zero ring, across which the phase changes by π. We see that the size of the ring increases as the spatial coherence is decreased. It should be noted that the spot size rapidly expands to its limiting value, and thus the ring radii in (b) and (c) are almost identical. Though we used a modal method for
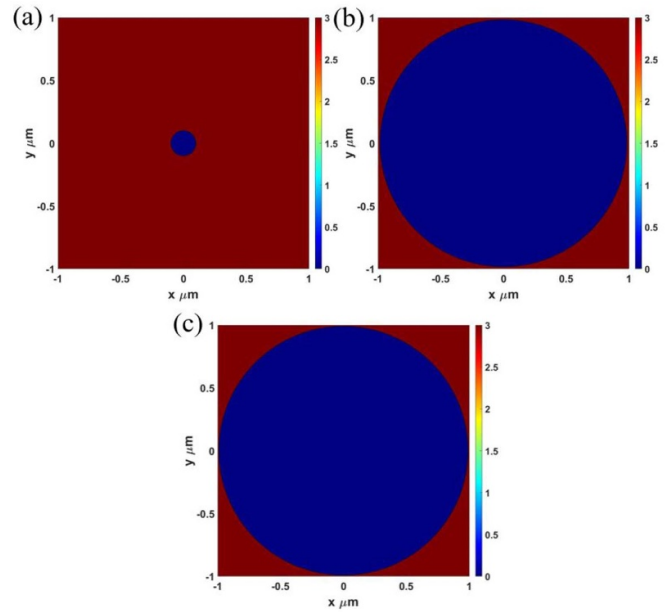
Figure 8. Phase of the cross-spectral density of the radial mode of the example demonstrated in figure 3: in this case $r_0 = 0.1\ \mu$m, $\sigma = 0.5\ \mu$m, and $(x_1, y_1) = (0.05, 0.0)$. In the figure, (a) $\mu = 1$, (b) $\mu = 0.5$, (c) $\mu = 0$.

introducing partial coherence, the result is similar to that of the beam wander model. The difference appears to arise due to the different functional forms of the modes in the radial ring case and the vortex case. It may be possible to produce rings that decrease in size as the coherence decreases, if more complicated combinations of modes are used.

7. Practical considerations

The model sources used in the aforementioned examples can doubtless be produced by a variety of methods, but it is worthwhile to give an example of how each can be generated, at least in principle.

A simple method for producing a beam satisfying the beam wander model is shown in figure 9(a), and was first described in [21]. A partially coherent illuminating field of Schell-model form, such as can be produced by passing light through a rotating ground glass plate, is passed through a vortex phase mask and then focused. The field in the focal plane will have the form of equation (5). Recently, it has been noted that partially coherent fields of the beam wander form possess unique topological characteristics on propagation [23]. To produce partially coherent superoscillatory fields, the simple vortex phase mask can be replaced by a mask producing the phase structure of equation (7).

The modal coherence model consists of a direct superposition of two LG modes of different orders with a global degree of coherence μ between them. Such a method could be produced, for example, by using a Mach–Zender interferometer, as shown in figure 9(b). In each arm of the interferometer, an spatial light modulator (SLM) can be used as a mirror and to
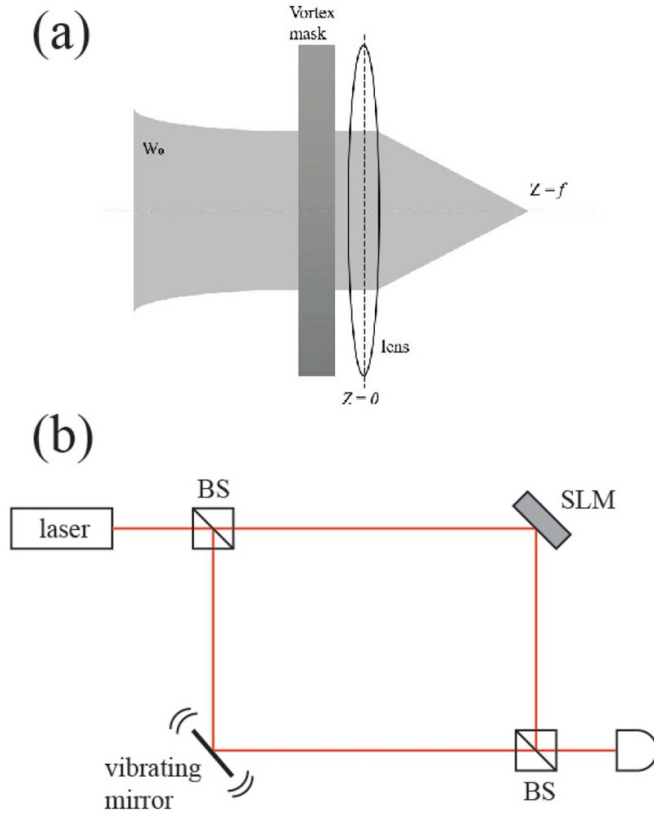
Figure 9. Simple experimental schemes for producing (a) the beam wander model, and (b) a partially coherent mode combination.

produce the desired mode. One mirror in one arm of the interferometer can be vibrated to produce a random phase fluctuation to produce partial coherence.

8. Concluding remarks

In this paper, we have explored the effect of partial coherence on superoscillatory behavior. Several different models were used to generate partial coherence, which have shown that it is possible in some cases for a decrease in coherence to decrease the spacing of superoscillatory zeros. The zeros manifest in the two-point cross-spectral density instead of the spectral density of the field, which means the rapid oscillations of the superoscillatory phase can be see even in locations where the light intensity is not close to zero. Sensing schemes which take advantage of interferometry to image objects and otherwise detect their structure could potentially benefit from such partially coherent superoscillations, and it is hoped that this work will stimulate further investigations into the physical and practical implications of these structures.

Data availability statement

All data that support the findings of this study are included within the article (and any supplementary files).

Acknowledgment

Dedication

This article is dedicated to the late Marat Soskin, who was a groundbreaking researcher in singular optics and also a delightful and insightful colleague and friend.

Appendix A. Cross-spectral density of the beam wander model

In this appendix, we will evaluate equation (5), showing the steps leading to the cross-spectral density presented in equation (8). We begin with a field of:

$$U(r) = (z + \Delta)(z - \Delta) \exp\left[-\frac{r^2}{2\sigma^2}\right]. \qquad (28)$$

In this field, σ is the beam width and Δ is the spacing of the zeros. The beam wander model is realized with a cross spectral density of:

$$W(\mathbf{r}_1, \mathbf{r}_2) = \int \tilde{U}(\mathbf{r}_1 - \mathbf{r}_0) U(\mathbf{r}_2 - \mathbf{r}_0) f(\mathbf{r}_0) d^2\mathbf{r}_0. \qquad (29)$$

$f(\mathbf{r}_0)$ is the probability density for the position of the axis and $\mathbf{r}_0$ is the transverse position on the axis. In this case, $f(\mathbf{r}_0)$ is:

$$f(\mathbf{r}_0) = \frac{1}{\pi\delta^2} \exp\left[-\frac{(x_0^2 + y_0^2)}{\delta^2}\right]. \qquad (30)$$

δ is the wander radius, which is the coherence parameter for our model. The cross-spectral density for our field is thus initially defined as:

$$
\begin{aligned}
W(\mathbf{r}_1, \mathbf{r}_2) = \frac{1}{\pi\delta^2} \int &(\tilde{z}_1 - \tilde{z}_0 + \Delta)(\tilde{z}_1 - \tilde{z}_0 - \Delta) \\
&\times (z_2 - z_0 + \Delta)(z_2 - z_0 - \Delta) \\
&\times \exp\left[-\frac{(\mathbf{r}_1 - \mathbf{r}_0)^2}{2\sigma^2}\right] \exp\left[-\frac{(\mathbf{r}_2 - \mathbf{r}_0)^2}{2\sigma^2}\right] \\
&\times \exp\left[-\frac{r_0^2}{\delta^2}\right] d^2 r_0.
\end{aligned}
\qquad (31)
$$

We begin simplifying by grouping the $\mathbf{r}_0$ terms together, giving:

$$
\begin{aligned}
W(\mathbf{r}_1, \mathbf{r}_2) = \frac{1}{\pi\delta^2} \int &\left[(\tilde{z}_1 - \tilde{z}_0)^2 - \Delta^2\right] \\
&\times \left[(z_2 - z_0)^2 - \Delta^2\right] \\
&\times \exp\left[-\frac{r_1^2}{2\sigma^2}\right] \exp\left[-\frac{r_2^2}{2\sigma^2}\right] \\
&\times \exp\left[\frac{(\mathbf{r}_1 + \mathbf{r}_2) \cdot \mathbf{r}_0}{\sigma^2}\right] \\
&\times \exp\left[-\left(\frac{1}{\sigma^2} + \frac{1}{\delta^2}\right) r_0^2\right] d^2 r_0.
\end{aligned}
\qquad (32)
$$

We introduce a new function Q, defined as:

$$Q = \frac{1}{\pi\delta^2}\exp\left[-\frac{r_1^2}{2\sigma^2}\right]\exp\left[-\frac{r_2^2}{2\sigma^2}\right]. \qquad (33)$$

In Cartesian coordinates, the cross-spectral density now has the form,

$$
\begin{aligned}
W(\mathbf{r}_1,\mathbf{r}_2) = Q \int & \left[[(x_1-x_0)-i(y_1-y_0)]^2 - \Delta^2\right] \\
& \times \left[[(x_2-x_0)+i(y_2-y_0)]^2 - \Delta^2\right] \\
& \times \exp\left[\frac{(x_1+x_2)x_0+(y_1+y_2)y_0}{\sigma^2}\right] \\
& \times \exp\left[-\left(\frac{1}{\sigma^2}+\frac{1}{\delta^2}\right)r_0^2\right] d^2r_0.
\end{aligned}
\qquad (34)
$$

Now we complete the square with respect to the x_0 and y_0 exponents with the introduction of the quantities:

$$A = \frac{1}{\sigma^2}+\frac{1}{\delta^2}, \qquad (35)$$

$$B_x = \frac{x_1}{\tilde{\sigma}^2}+\frac{x_2}{\sigma^2}, \qquad (36)$$

$$B_y = \frac{y_1}{\tilde{\sigma}^2}+\frac{y_2}{\sigma^2}, \qquad (37)$$

and the definition of a new function:

$$Q_1 = Q\exp\left[\frac{B_x^2}{4A}\right]\exp\left[\frac{B_y^2}{4A}\right]. \qquad (38)$$

This process reduces the cross-spectral density to the form:

$$
\begin{aligned}
W(\mathbf{r}_1,\mathbf{r}_2) = Q_1 \int & \left[[(x_1-x_0)-i(y_1-y_0)]^2 - \Delta^2\right] \\
& \times \left[[(x_2-x_0)+i(y_2-y_0)]^2 - \Delta^2\right] \\
& \times \exp\left[-A\left(x_0-\frac{B_x}{2A}\right)^2\right] \\
& \times \exp\left[-A\left(y_0-\frac{B_y}{2A}\right)^2\right] d^2r_0.
\end{aligned}
\qquad (39)
$$

We now do the coordinate transformation,

$$X = x_0 - \frac{B_x}{2A}, \qquad (40)$$

$$Y = y_0 - \frac{B_y}{2A}, \qquad (41)$$

providing us with a cross-spectral density defined as:

$$
\begin{aligned}
W(\mathbf{r}_1,\mathbf{r}_2) = Q_1 \int & \left[\left[\left(x_1-X-\frac{B_x}{2A}\right)-i\left(y_1-Y-\frac{B_y}{2A}\right)\right]^2-\Delta^2\right] \\
& \times \left[\left[\left(x_2-X-\frac{B_x}{2A}\right)+i\left(y_2-Y-\frac{B_y}{2A}\right)\right]^2-\Delta^2\right] \\
& \times \exp\left[-AX^2\right]\exp\left[-AY^2\right]dXdY.
\end{aligned}
\qquad (42)
$$

To evaluate the integrals, we define the terms:

$$
\begin{aligned}
-C_{1x} = -x_1 + \frac{B_x}{2A}, \quad -C_{2x} = -x_2 + \frac{B_x}{2A}, \\
-C_{1y} = -y_1 + \frac{B_y}{2A}, \quad -C_{2y} = -y_2 + \frac{B_y}{2A}.
\end{aligned}
\qquad (43)
$$

We additionally define the following complex quantities,

$$C_i = C_{ix}+iC_{iy}, Z = X+iY, \tilde{Z} = X-iY. \qquad (44)$$

Applying all of the above definitions, and plugging them into the cross-spectral density, we simplify our integral to the form,

$$
\begin{aligned}
W(\mathbf{r}_1,\mathbf{r}_2) = Q_1 \int & e^{-A(X^2+Y^2)}\left[(\tilde{C}_1+\tilde{Z})^2-\Delta^2\right] \\
& \times \left[(C_2+Z)^2-\Delta^2\right]dXdY.
\end{aligned}
\qquad (45)
$$

We introduce a final pair of constants,

$$\tilde{D}_1 = \tilde{C}_1^2 - \Delta^2, D_2 = C_2^2 - \Delta^2. \qquad (46)$$

All components of the integrand are now in powers of Z and $\tilde{Z}$. By converting to polar coordinates, we find that a number of components of the integral evaluate to zero, and we are left with:

$$W(\mathbf{r}_1,\mathbf{r}_2) = Q_1 \int \left[r^4+4\tilde{C}_1 C_2 r^2+\tilde{D}_1 D_2\right] r\,dr\,d\phi. \qquad (47)$$

This integral can be readily solved, allowing us to write our final expression for the cross-spectral density as:

$$W(\mathbf{r}_1,\mathbf{r}_2) = Q_1 \left[\frac{1}{A^3}+\frac{2\tilde{C}_1 C_2}{A^2}+\frac{\tilde{D}_1 D_2}{2A}\right]. \qquad (48)$$

ORCID iD

Greg Gbur ⓘ https://orcid.org/0000-0002-3100-5985

References

[1] Berry M *et al* 2019 Roadmap on superoscillations *J. Opt.* **21** 053002

[2] Gbur G 2019 Using superoscillations for superresolved imaging and subwavelength focusing *Nanophotonics* **8** 205–25

[3] Chremmos I and Fikioris G 2015 Superoscillations with arbitrary polynomial shape *J. Phys. A: Math. Theor.* **48** 265204

[4] Smith M K and Gbur G 2016 Construction of arbitrary vortex and superoscillatory fields *Opt. Lett.* **41** 4979–82

[5] Gbur G J 2017 *Singular Optics* (Boca Raton, FL: CRC Press)

[6] Wong A M H and Eleftheriades G V 2011 Sub-wavelength focusing at the multi-wavelength range using superoscillations: an experimental demonstration *IEEE Trans. Antennas Propag.* **59** 4766–76

[7] Rogers E T F, Lindberg J, Roy T, Savo S, Chad J E, Dennis M R and Zheludev N I 2012 A super-oscillatory lens optical microscope for subwavelength imaging *Nat. Mater.* **11** 432–5

[8] Rogers E T F, Savo S, Lindberg J, Roy T, Dennis M R and Zheludev N I 2013 Super-oscillatory optical needle *Appl. Phys. Lett.* **102** 031108

[9] Roy T, Rogers E T F, Yuan G and Zheludev N I 2014 Point spread function of the optical needle super-oscillatory lens *Appl. Phys. Lett.* **104** 231109

[10] Smith M K and Gbur G 2020 Mathematical method for designing superresolution lenses using superoscillations *Opt. Lett.* **45** 1854–7

[11] Gbur G, Visser T D and Wolf E 2004 Hidden' singularities in partially coherent wavefields *J. Opt. A: Pure Appl. Opt.* **6** S239–42

[12] Berry M V 2016 Suppression of superoscillations by noise *J. Phys. A: Math. Theor.* **50** 025003

[13] Katzav E, Perlsman E and Schwartz M 2016 Yield statistics of interpolated superoscillations *J. Phys. A: Math. Theor.* **50** 025001

[14] Maleev I D, Palacios D M, Marathay A S and Swartzlander G A Jr 2004 Spatial correlation vortices in partially coherent light: theory *J. Opt. Soc. Am.* B **21** 1895–900

[15] Palacios D M, Maleev I D, Marathay A S and Swartzlander G A Jr 2004 Spatial correlation singularity of a vortex field *Phys. Rev. Lett.* **92** 143905

[16] Gbur G and Visser T D 2003 Coherence vortices in partially coherent beams *Opt. Commun.* **222** 117–25

[17] Korotkova O and Gbur G 2020 Chapter four—applications of optical coherence theory *A Tribute to Emil Wolf* (Progress in Optics) vol 65 ed T D Visser (Amsterdam: Elsevier) pp 43–104

[18] Mandel L and Wolf E 1995 *Optical Coherence and Quantum Optics* (Cambridge: Cambridge University Press)

[19] Dennis M R, Hamilton A C and Courtial J 2008 Superoscillation in speckle patterns *Opt. Lett.* **33** 2976–8

[20] Berry M V 2019 Superoscillations and leaky spectra *J. Phys. A: Math. Theor.* **52** 015202

[21] Gu Y and Gbur G 2009 Topological reactions of optical correlation vortices *Opt. Commun.* **282** 709–16

[22] Stahl C S D and Gbur G 2017 Partially coherent vortex beams of arbitrary order *J. Opt. Soc. Am.* A **34** 1793–9

[23] Zhang Y, Cai Y and Gbur G 2020 Partially coherent vortex beams of arbitrary radial order and a van Cittert–Zernike theorem for vortices *Phys. Rev.* A **101** 043812